AIP | Applied Physics Letters

Broadband enhanced transmission of acoustic waves through serrated metal gratings

Dong-Xiang Qi, Yu-Qiang Deng, Di-Hu Xu, Ren-Hao Fan, Ru-Wen Peng, Ze-Guo Chen, Ming-Hui Lu, X. R. Huang, and Mu Wang

Citation: Applied Physics Letters **106**, 011906 (2015); doi: 10.1063/1.4905340
View online: http://dx.doi.org/10.1063/1.4905340
View Table of Contents: http://scitation.aip.org/content/aip/journal/apl/106/1?ver=pdfcov
Published by the AIP Publishing

Broadband enhanced transmission of acoustic waves through serrated metal gratings

Dong-Xiang Qi,[1,2,a)] Yu-Qiang Deng,[1] Di-Hu Xu,[1] Ren-Hao Fan,[1] Ru-Wen Peng,[1,a)] Ze-Guo Chen,[1] Ming-Hui Lu,[1] X. R. Huang,[3] and Mu Wang[1]
[1]*National Laboratory of Solid State Microstructures and School of Physics, Collaborative Innovation Center of Advanced Microstructures, Nanjing University, Nanjing 210093, China*
[2]*School of Science, Jiangnan University, Wuxi 214122, China*
[3]*Advanced Photon Source, Argonne National Laboratory, Argonne, Illinois 60439, USA*

(Received 24 September 2014; accepted 19 December 2014; published online 9 January 2015)

In this letter, we have demonstrated that serrated metal gratings, which introduce gradient coatings, can give rise to broadband transmission enhancement of acoustic waves. Here, we have experimentally and theoretically studied the acoustic transmission properties of metal gratings with or without serrated boundaries. The average transmission is obviously enhanced for serrated metal gratings within a wide frequency range, while the Fabry-Perot resonance is significantly suppressed. An effective medium hypothesis with varying acoustic impedance is proposed to analyze the mechanism, which was verified through comparison with finite-element simulation. The serrated boundary supplies gradient mass distribution and gradient normal acoustic impedance, which could efficiently reduce the boundary reflection. Further, by increasing the region of the serrated boundary, we present a broadband high-transmission grating for wide range of incident angle. Our results may have potential applications to broadband acoustic imaging, acoustic sensing, and acoustic devices. © *2015 AIP Publishing LLC*. [http://dx.doi.org/10.1063/1.4905340]

The manipulation of waves through artificial materials is an intriguing subject that has been extensively developed over the past decade.[1–20] Through ingenious design, material properties could be extended to unnatural and fascinating regions for acoustic waves, such as negative refraction,[1–4] subwavelength imaging,[5–8] acoustic cloaking,[9–12] extraordinary transmission,[13–17] and so on. Extending the broadband working range is the current challenge for further developments, and has already attracted intense attentions. For example, simultaneously exciting adjacent multiple modes through complex structures could exceed the bandwidth limit of a single resonant mode.[21–23] Moreover, quasi-periodic structure could excite multiple diffractions, which could broaden the working frequency range of acoustic asymmetric transmission.[24] Very recently, gradient-index structure was utilized to efficiently inhibit wave reflection to obtain broadband high transmission.[25,26] Related researches have broad application potentials in subwavelength imaging, asymmetric transmission,[24,27] broadband sensing, and so on.

The broadband properties of acoustic transmission though gratings have already been demonstrated under oblique incidence, which could be explained through effective acoustic impedance matching.[28,29] However, this phenomenon is very sensitive to large oblique incident angles, limiting further development. Gradient-index structures could also be utilized for broadband antireflection,[25,26] planar lens,[30,31] and broadband asymmetric transmission.[27] To achieve gradient-index structures, people have employed the phononic crystals with spatially varying filling fractions.[27,32] However, to some extent multiple-scattering-based mechanism limits the working frequency region of acoustic waves in phononic crystals.

In this letter, we studied four metal gratings and demonstrated that serrated boundaries lead to broadband transmission enhancement of acoustic waves. Physically the serrated boundary region supplies a gradient transition layer between the air and the grating, effectively reducing the interface reflection. Furthermore, we enlarge the gradient layer by increasing the serrated boundary region, and propose a serrated grating with broadband high transmission for wide range of incident angles. This research may provide some inspiration for gradient structure design, which may be applied in broadband acoustic devices.

Here, we studied four different metal gratings with and without serrated boundaries, which are labeled samples I, II, III, and IV, as shown in Fig. 1. Then, a beam of acoustic wave is incident on the gratings. As shown in Fig. 1, samples I and II are metal gratings with smooth boundaries, while samples III and IV are the corresponding gratings with serrated boundaries. Sample I is a vertical smooth grating (Fig. 1(a1)), where the period and the width of the slits are $d = 5.5$ mm and $w = 2.5$ mm, respectively, and the thickness is $h = 20$ mm. Sample II is an oblique smooth grating (Fig. 1(b1)). The metal strips are stacked under the oblique angle $\theta = 32^{\circ}$, while the boundary is smooth. Sample III is a vertical serrated grating (Fig. 1(c1)), and could be fabricated by adding serrated triangles (1.87 mm height with 58° vertex) to sample I. Sample IV is an oblique serrated grating (Fig. 1(d1)), which utilized the same steel strips as sample I but stacked under tilt angle of $\theta = 32^{\circ}$. The serrated boundary regions of the gratings are relatively small, so these four gratings have nearly the same filling ratio.

The four gratings were fabricated through sequentially stacking steel strips and were immersed in air. An acoustic

[a)]Authors to whom correspondence should be addressed. Electronic addresses: dongxiang87@gmail.com and rwpeng@nju.edu.cn

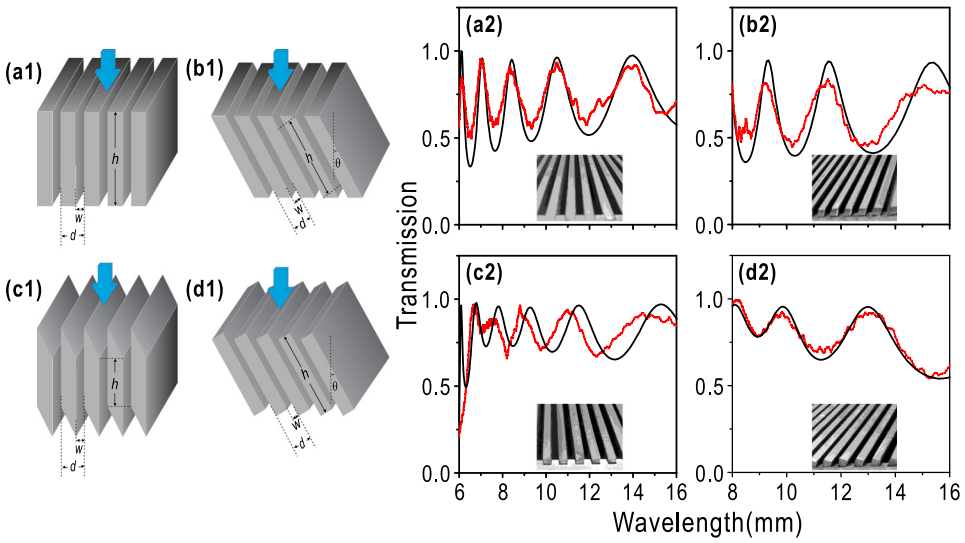

FIG. 1. (a1)–(d1) show the schematic pictures of four gratings, while (a2)–(d2) show the transmission spectra of four gratings. (a1) and (a2) sample I: vertical smooth grating; (b1) and (b2) sample II: oblique smooth grating; (c1) and (c2) sample III: vertical serrated grating; (d1) and (d2) sample IV: oblique serrated grating. For all gratings, $h = 20$ mm, $d = 5.5$ mm, $w = 2.5$ mm, and $\theta = 32°$, respectively. On the right panel, red lines correspond to the experimental results while black lines correspond to the finite-element simulations. The insets are photos of steel gratings.

wave beam was incident on the gratings and the transmission spectra were measured by the analysis package of the 3560C Brüel & Kjær Pulse Sound and Vibration Analyzers. We verified the results with finite-element simulations. The transmission spectra of the four gratings obtained from experiments and finite-element simulations are shown in Figs. 1(a2)–1(d2). The transmission peaks and dips originate from the Fabry-Perot interferences. Comparing to sample I, the average transmission within the 6–16 mm wavelength range is enhanced (from 0.71 to 0.80) for sample III. The two gratings have nearly the same geometry, except for the thin serrated boundary. However, the Fabry-Perot effect is obviously suppressed for the serrated boundary, leading to broadband transmission enhancement. Similar results could also be obtained for sample II and sample IV. With the serrated boundary in sample IV, the Fabry-Perot effect is suppressed, and the average transmission is obviously enhanced (from 0.61 to 0.80) within the 8–16 mm wavelength range compared to sample II. Moreover, serrated boundary region was found to play a vital role in the broadband enhanced transmission by inhibiting Fabry-Perot interference.

The angular transmission spectra of the four gratings by finite-element simulations are shown in Fig. 2. Comparing gratings with and without the serrated boundary, the Fabry-Perot effect is weakened, and the averaged transmission within 4–30 mm wavelength range is enhanced for different incident angles (at least 10% enhancement between $0^o \leq \theta \leq 38^o$). As the incident angle increased, broadband flat transmission could appear at optimal incident angle of $\theta_f \cong \cos^{-1}[(d-w)/d]$.[28] As all four gratings have nearly the same filling ratio and the serrated boundary is thin enough to be neglected, the broadband flat transmission can be observed at nearly the same optimal angle (63^o) incidence (shown by the white dotted lines in Fig. 2). We found that the serrated boundary and proper incident angle could both suppress the Fabry-Perot effect and enhance the transmission. Compared with tuning the incident angle, the serrated boundary is more suitable for practical applications.

Because the grating periods are less than wavelength of the acoustic waves, we utilized an effective medium theory to characterize the gratings. Taking the gratings as plates, we could achieve the relative effective index n and impedance ξ from the complex transmission and reflection coefficients for normal incidence,[33] respectively. Here, $n = c_0/c_r$ and $\xi = \rho_r c_r/\rho_0 c_0$, where ρ_0 and c_0 are the mass density and sound velocity of air, respectively, while ρ_r and c_r are the effective mass density and velocity of gratings, respectively. The calculated real part of n and ξ are shown in Fig. 3. For samples I and III, $\mathrm{Re}(n)$ is not sensitive to the wavelength and approximately equals 1, while $\mathrm{Re}(\xi)$ has different slopes corresponding to the different impedance ratio and grating transmissions. While for samples II and IV, $\mathrm{Re}(n)$ is not sensitive to the wavelength, but $\mathrm{Re}(n)$ is larger than 1 for the slope guide path of acoustic waves. From the $\mathrm{Re}(n)$ performance, acoustic waves are thought to propagate along the slit directions inside the grating and could be described by zero-order guided mode, regardless of serrated boundary. To further analyze the serrated boundary effects, we propose an effective medium hypothesis with varying acoustic impedance along the propagation direction.

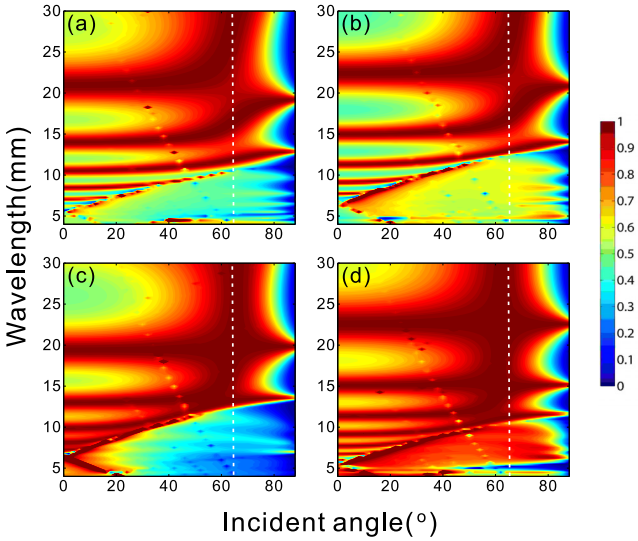

FIG. 2. Angular transmission spectra obtained by finite-element simulations: (a) sample I: vertical smooth grating; (b) sample II: oblique smooth gratings; (c) sample III: vertical serrated grating; and (d) sample IV: oblique serrated grating. The optimal angles (indicated by white dotted lines) for four gratings are all around 63°.

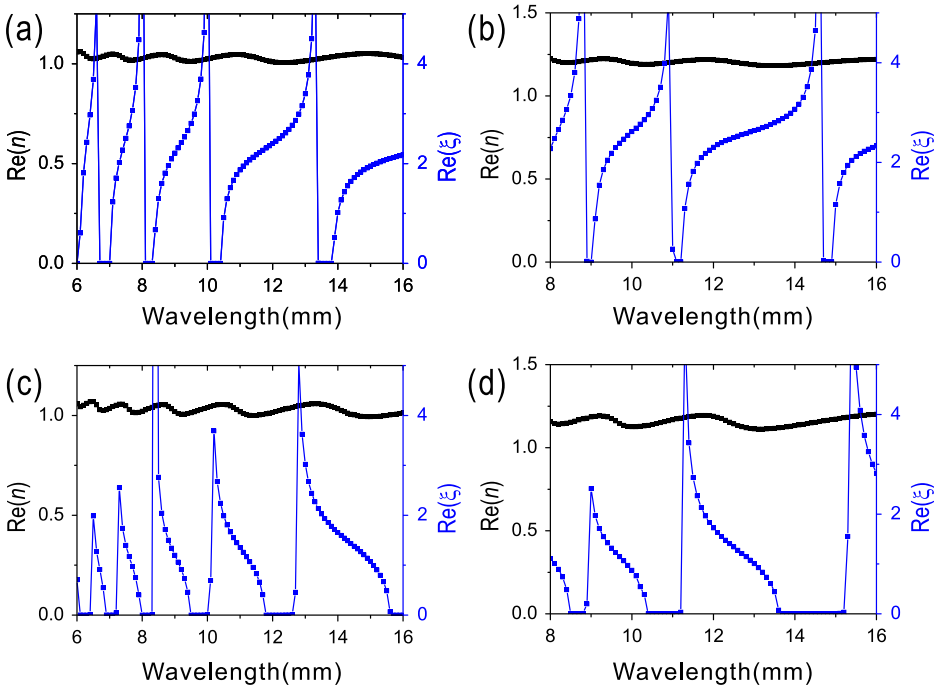

FIG. 3. The relative effective index (black) and impedance (blue) vary with wavelength: (a) sample I: vertical smooth grating; (b) sample II: oblique smooth grating; (c) sample III: vertical serrated grating; and (d) sample IV: oblique serrated grating.

We then perform additional calculations based on the effective medium hypothesis to analyze the broadband enhanced transmission phenomena in serrated gratings. The serrated boundary is thought to supply a gradient layer with varying effective acoustic impedance. To obtain the transmission properties through material interface, we could analyze the normal acoustic impedance ratio between the two materials. For normal incidence, the effective normal acoustic impedance (the ratio of pressure and normal velocity) of air is $Z_{air\_norm} = \rho_0 c_0$, where ρ_0 and c_0 are mass density and acoustic velocity of air, respectively. Inside acoustic gratings, the zero-order guided mode is a good approximation for describing acoustic propagation through the gratings. Consequently, acoustic waves are thought to propagate along the slits direction inside the grating regardless of the incident angle.

For gratings, the effective velocity could be set to the constant c_r based on above results in Fig. 3, while the effective mass density equals $\rho_0 d/w(z)$, where $w(z)$ is the local width of the slits along the propagation direction (z coordinate). Then, the effective normal acoustic impedance of the grating is given as follows:

$$Z_{grating\_norm} = \rho_0 c_r d/w(z). \quad (1)$$

Based on the above effective medium hypothesis, we can perform analytical calculations on the effective acoustic impedance through the metal gratings (as shown in Fig. 4). For sample I, the effective normal acoustic impedance distribution of the air and grating is shown in Fig. 4(b). The gray regions correspond to the gratings. As shown in Fig. 4(b), there is a sharp impedance change at the boundary. For sample III, the effective normal acoustic impedance distribution along the z direction is shown in Fig. 4(d). We find a gradient transition layer at the boundary, where the normal acoustic impedance gradually increased from air to grating. This gradient transition layer is the physical origin of the broadband antireflection.

To further verify the rationality of effective medium hypothesis, we also calculated the transmission spectra and compared them with the simulated results shown in Figs. 4(a) and 4(c). To calculate the transmission spectra based on effective medium hypothesis, we already discussed the effective normal acoustic impedance. In addition, multiple diffractive waves could be excited at the grating boundary, adding an extra phase shift. As a result, the effective thickness of the grating should be $h_e = h + \Delta h(\omega)$. To simplify the discussion, we set the fitting coefficient h_e to be frequency independence. Then, we utilized the transfer matrix method to calculate the transmission spectra. For gradient transition layer, the effective normal acoustic impedance varied continuously. To solve this problem, we divided the gradient transition layer into N thin homogeneous layers. The pressure field in each layer can be expressed as

$$p_n(z) = p_t^n \exp(ikz) + p_r^n \exp(-ikz) \quad (n = 1, 2, \ldots N), \quad (2)$$

where $k = \omega/c_0$. The pressure field above and below the grating can be expressed as

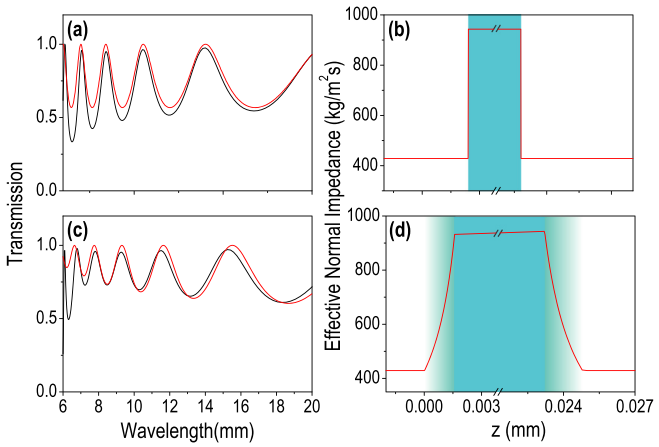

FIG. 4. (a) and (c) The transmission spectra of vertical gratings with smooth and serrated boundaries, respectively. Here, black lines correspond to the finite-element simulation while red lines correspond to the calculations based on effective medium hypothesis. (b) and (d) The effective acoustic normal impedance distributions along the z-direction for vertical gratings with smooth and serrated boundaries, respectively.

$$\begin{cases} p_0 = p_t^0 \exp(ikz) + p_r^0 \exp(-ikz), \\ p_{N+1} = p_t^{N+1} \exp(ikz). \end{cases} \quad (3)$$

Considering the pressure continuum and velocity continuum conditions, we find

$$H_n(z_n)m_n = H_{n+1}(z_n)m_{n+1} \quad (n = 0, 1, 2 \ldots N+1). \quad (4)$$

Here, $H_n(z) = \begin{pmatrix} \exp(ikz_n) & \exp(-ikz_n) \\ \exp(ikz_n)/Z_n & -\exp(-ikz_n)/Z_n \end{pmatrix}$, and $m_n = \begin{pmatrix} p_t^n \\ p_r^n \end{pmatrix}$, where z_n and Z_n are the coordinate and effective normal acoustic impedance of the n-th layer, respectively, and $z_0 = 0$. Through matrix operation, we obtain

$$\begin{pmatrix} p_t^{N+1} \\ 0 \end{pmatrix} = [H_{N+1}(z_N)]^{-1} H_N(z_N) \ldots [H_{n+1}(z_n)]^{-1} \times H_n(z_n) \ldots [H_1(z_0)]^{-1} H_0(z_0) \begin{pmatrix} p_t^0 \\ p_r^0 \end{pmatrix}. \quad (5)$$

Here, we set $p_t^0 = 1$, and then, the transmittance of the acoustic wave is given by

$$t = |p_t^{N+1}|^2. \quad (6)$$

For sample I, the calculation is simple and the results have already been discussed.[14] As shown in Fig. 4(a), the calculation result based on effective medium hypothesis agrees well with simulated result in long wavelength region. In the short wavelength region, the deviation increased with shorter wavelengths due to the enhanced diffractive effect. While for sample III, the effective normal acoustic impedance varied continuously in the gradient transition layer as in Fig. 4(c). The calculations based on effective medium hypothesis agree well with the finite-element simulation. Unlike sample I, broadband enhanced transmission can be observed in sample III. For samples II and IV, because of the more complex boundary conditions, the frequency independent effective thickness settings could not work very well and are not shown here. However, the gradient transition layer could also explain the broadband enhanced transmission phenomenon. We conclude that our effective acoustic impedance settings are reasonable for vertical serrated gratings. The broadband enhanced transmission phenomena are due to the gradient transition layers.

From the above discussion, we know the gradient transition layer plays an important role in the broadband enhanced transmission. Therefore, we could enlarge the gradient transition layers to obtain a better broadband transmission enhancement. As shown in Fig. 5, we designed a metal grating by increasing the thickness of the serrated boundary region to one-third of the total thickness without changing the total filling ratio compared to sample I. Broadband high transmission for normal incidence is shown in Fig. 5(a). The thicker gradient transition layer could slow the acoustic impedance change, inducing a better antireflection effect. Through the angular transmission spectra obtained by finite-element simulation (Fig. 5(c)), we found that broadband high transmission could be realized in a large incident angle region (between $0^o \le \theta \le 40^o$, the average transmission within the 6–25 mm wavelength range is greater than 0.85). At higher incident angles, broadband high transmission disappeared, and resonant transmission peaks occurred. To explain these phenomena, we could also utilize effective medium hypothesis to analyze the transmission properties.

As discussed above, acoustic waves are thought to propagate along the slit direction inside the grating regardless of the incident angle. Thus, for oblique incidence, the effective normal acoustic impedance of the grating is the same as the normal incidence: $Z_{grating\_norm} = \rho_0 c_r d/w(z)$. For air, the

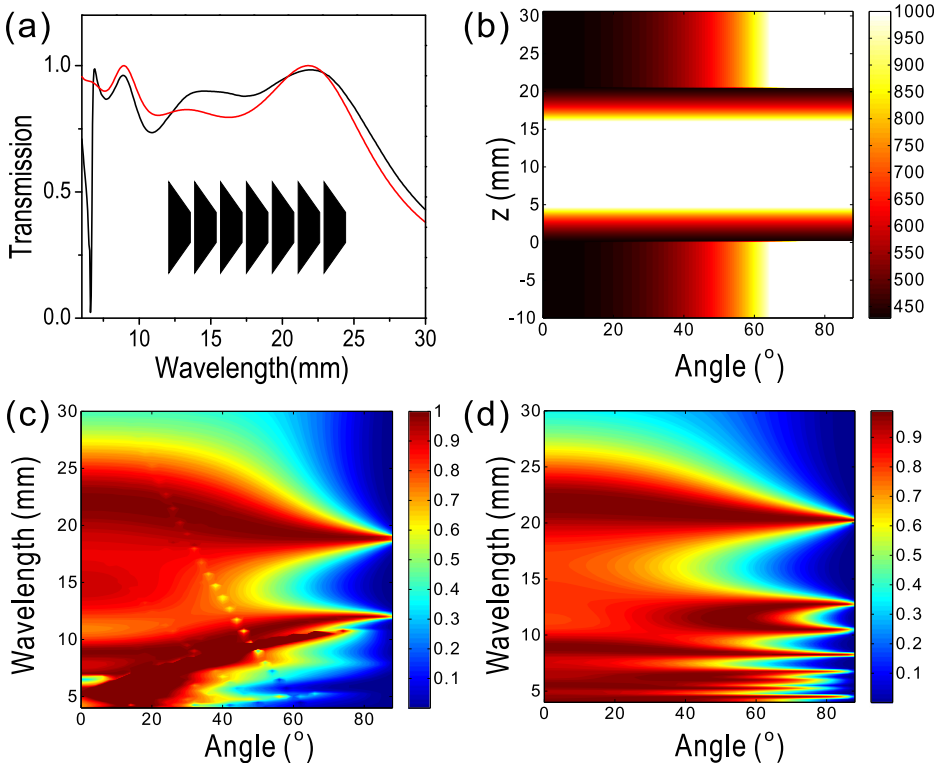

FIG. 5. Increasing the gradient boundary region. (a) Transmission spectra for normal incidence obtained with finite-element simulation (black line) and calculations (red line) based on the effective medium hypothesis. The inset is schematic picture of grating. (b) Spatial distribution of the effective normal acoustic impedance of the grating. The color bar corresponds to the effective acoustic impedance. (c) and (d) The angular transmission spectra obtained with finite-element simulation and calculations based on the effective medium hypothesis, respectively.

effective normal acoustic impedance is $Z_{air\_norm} = \rho_0 c_0 / \cos\theta$ for incident angle θ. The angular effective normal acoustic impedance distribution is shown in Fig. 5(b). Based on these settings, we could calculate the angular transmission spectra through transfer matrix method shown in Fig. 5(d). We found good agreement between simulated results and the results calculated through effective acoustic impedance method shown in Figs. 5(c) and 5(d), respectively, which again verified the effective settings. We observed deviations in the short wavelength region and at high incident angles, because of the additional diffractive effects at those conditions. As shown in Fig. 5(b), for small angle ($\theta < 40^o$) incidence, the gradient boundary layer acts as a good air-to-grating transition layer. The effective normal acoustic impedance of air did not significantly vary with the incident angle in this region. Moreover, the effective normal acoustic impedance distribution varied gradually along the z-direction. As a result, the gradient boundary layer could effectively reduce the reflection at the interfaces inducing angle-insensitive broadband high transmission. On the other hand, for higher angle incidence, the effective normal acoustic impedance of air changed significantly, and sharp changes appeared at the interfaces. These sharp changes of the effective normal acoustic impedance would induce high reflection, resulting in obvious Fabry-Perot resonant transmission. Unlike the samples in Fig. 2, the serrated boundary here could not be neglected, so the effective normal acoustic impedance matching could not be satisfied, thereafter the broadband high transmission could not happen at large incident angle (as shown in Fig. 5). Therefore, by increasing the serrated boundary region, we could design a grating with angle-insensitive broadband high transmission, which could be understood by the effective medium hypothesis.

In summary, we studied the acoustic transmission properties of four gratings, and experimentally found that broadband enhanced transmission occurred through serrated gratings for normal incidence. Through the angular transmission spectra obtained by the finite-element simulation, we show that the Fabry-Perot effect and the average transmission could be affected by the serrated boundary within wide incident angles. Furthermore, the effective medium hypothesis was utilized to analyze the broadband enhanced transmission phenomena. The serrated boundary supplies a gradient acoustic impedance distribution, which could effectively reduce the boundary acoustic reflection and enhance the total transmission. Because the serrated boundary plays an important role in transmission enhancement, we proposed a grating with an enlarged serrated boundary region without changing the total filling ratio. Broadband high transmission could be seen for wide range of incident angles. Our studies may have potential applications in acoustic imaging, acoustic cloaking, and acoustic device design.

This work was supported by the Ministry of Science and Technology of China (Grant Nos. 2012CB921502 and 2010CB630705), the National Natural Science Foundation of China (Grant Nos. 11034005, 61475070, 11474157, and 11321063), the Fundamental Research Funds for the Central Universities (Grant No. JUSRP11401), and the Natural Science Foundation of Jiangsu Province of China (Grant No. BK20140127). X.R.H. was supported by the U.S. Department of Energy, Office of Science, Office of Basic Energy Sciences, under Contract No. DE-AC02-06CH11357.

[1]N. Fang, D. Xi, J. Xu, M. Ambati, W. Srituravanich, C. Sun, and X. Zhang, Nat. Mater. **5**, 452 (2006).
[2]M.-H. Lu, C. Zhang, L. Feng, J. Zhao, Y.-F. Chen, Y.-W. Mao, J. Zi, Y.-Y. Zhu, S.-N. Zhu, and N.-B. Ming, Nat. Mater. **6**, 744 (2007).
[3]J. Christensen and F. Javier García de Abajo, Phys. Rev. Lett. **108**, 124301 (2012).
[4]M. Yang, G. Ma, Z. Yang, and P. Sheng, Phys. Rev. Lett. **110**, 134301 (2013).
[5]A. Sukhovich, B. Merheb, K. Muralidharan, J. O. Vasseur, Y. Pennec, P. A. Deymier, and J. H. Page, Phys. Rev. Lett. **102**, 154301 (2009).
[6]Z. He, F. Cai, Y. Ding, and Z. Liu, Appl. Phys. Lett. **93**, 233503 (2008).
[7]J. Li, L. Fok, X. Yin, G. Bartal, and X. Zhang, Nat. Mater. **8**, 931 (2009).
[8]J. Zhu, J. Christensen, J. Jung, L. Martin-Moreno, X. Yin, L. Fok, X. Zhang, and F. J. Garcia-Vidal, Nat. Phys. **7**, 52 (2011).
[9]H. Chen and C. T. Chan, Appl. Phys. Lett. **91**, 183518 (2007).
[10]M. Farhat, S. Guenneau, and S. Enoch, Phys. Rev. Lett. **103**, 024301 (2009).
[11]S. Zhang, C. Xia, and N. Fang, Phys. Rev. Lett. **106**, 024301 (2011).
[12]X. Zhu, B. Liang, W. Kan, X. Zou, and J. Cheng, Phys. Rev. Lett. **106**, 014301 (2011).
[13]H. Estrada, P. Candelas, A. Uris, F. Belmar, F. J. García de Abajo, and F. Meseguer, Phys. Rev. Lett. **101**, 084302 (2008).
[14]J. Christensen, L. Martin-Moreno, and F. J. Garcia-Vidal, Phys. Rev. Lett. **101**, 014301 (2008).
[15]C. Qiu, S. Xu, M. Ke, and Z. Liu, Phys. Rev. B **90**, 094109 (2014).
[16]Z. Liang and J. Li, Phys. Rev. Lett. **108**, 114301 (2012).
[17]Z. He, H. Jia, C. Qiu, S. Peng, X. Mei, F. Cai, P. Peng, M. Ke, and Z. Liu, Phys. Rev. Lett. **105**, 074301 (2010).
[18]X. R. Huang, R. W. Peng, and R. H. Fan, Phys. Rev. Lett. **105**, 243901 (2010).
[19]A. Alù, G. D'Aguanno, N. Mattiucci, and M. J. Bloemer, Phys. Rev. Lett. **106**, 123902 (2011).
[20]R. H. Fan, R. W. Peng, X. R. Huang, J. Li, Y. Liu, Q. Hu, M. Wang, and X. Zhang, Adv. Mater. **24**, 1980 (2012).
[21]Y. Zhao, Q. Hao, Y. Ma, M. Lu, B. Zhang, M. Lapsley, I. Khoo, and T. J. Huang, Appl. Phys. Lett. **100**, 053119 (2012).
[22]L.-H. Zhu, M.-R. Shao, R.-W. Peng, R.-H. Fan, X.-R. Huang, and M. Wang, Opt. Express **21**, A313 (2013).
[23]L. Wen, F. Sun, and Q. Chen, Appl. Phys. Lett. **104**, 151106 (2014).
[24]C. Li, M. Ke, Y. Ye, S. Xu, C. Qiu, and Z. Liu, Appl. Phys. Lett. **105**, 023511 (2014).
[25]W. H. Southwell, Opt. Lett. **8**, 584 (1983).
[26]X. Li, L. Xue, and Y. Han, J. Mater. Chem. **21**, 5817 (2011).
[27]R.-Q. Li, B. Liang, Y. Li, W.-W. Kan, X.-Y. Zou, and J.-C. Cheng, Appl. Phys. Lett. **101**, 263502 (2012).
[28]D.-X. Qi, R.-H. Fan, R.-W. Peng, X.-R. Huang, M.-H. Lu, X. Ni, Q. Hu, and M. Wang, Appl. Phys. Lett. **101**, 061912 (2012).
[29]G. D'Aguanno, K. Q. Le, R. Trimm, A. Alù, N. Mattiucci, A. D. Mathias, N. Aközbek, and M. J. Bloemer, Sci. Rep. **2**, 340 (2012).
[30]H. Han, L. Wu, X. Tian, D. Li, M. Yin, and Y. Wang, J. Appl. Phys. **112**, 114913 (2012).
[31]S.-C. S. Lin, B. R. Tittmann, and T. J. Huang, J. Appl. Phys. **111**, 123510 (2012).
[32]D. Torrent, A. Hakansson, F. Cervera, and J. Sanchez-Dehesa, Phys. Rev. Lett. **96**, 204302 (2006).
[33]V. Fokin, M. Ambati, C. Sun, and X. Zhang, Phys. Rev. B **76**, 144302 (2007).